

Chapter 10

The Shanghai Superintense Ultrafast Laser Facility (SULF) Project



Zebiao Gan, Lianghong Yu, Cheng Wang, Yanqi Liu, Yi Xu, Wenqi Li, Shuai Li, Linpeng Yu, Xinliang Wang, Xinyan Liu, Junchi Chen, Yujie Peng, Lu Xu, Bo Yao, Xiaobo Zhang, Lingru Chen, Yunhai Tang, Xiaobin Wang, Dinjun Yin, Xiaoyan Liang, Yuxin Leng, Ruxin Li, and Zhizhan Xu

Abstract We report the recent progress on the Shanghai Superintense Ultrafast Laser Facility (SULF) project. The schematic design of SULF is described. The upgrade information from SULF laser prototype to SULF 10 PW laser user facility is presented in detail. A high contrast front is developed to generate high-quality clean seed pulses which are then stretched to about 2 ns by a new double-grating Öffner stretcher. A Dazzler is used to control the high-order phase distortions and shape the spectrum of the laser pulses simultaneously. The laser pulses are amplified to 7 J energy in the 1 Hz pre-amplifiers system before injected into the three stages large aperture main amplifiers system. The first two main amplifiers are pumped by five commercial lasers which can be operated at 1 shot/min. The final main amplifier is pumped by six home-built high energy frequency doubled Nd:glass lasers at a repetition rate of 1 shot/3 min. The final amplifier output energy is ~408 J with high stability under a pump energy of ~530 J. Compressed pulse duration of the amplified laser and the total transport efficiency for compression is measured to be 22.4 fs and 70.52% respectively. The experimental results demonstrate that SULF user facility has the capacity to deliver 10 PW peak power femtosecond pulses.

10.1 Introduction

The invention and rapid development of high-intensity, ultra-short lasers have undoubtedly revolutionized the scientific world. Due to their ability to concentrate a large amount of energy within extremely short time intervals, as well as coherent laser light can be focused to the diffraction limit, people can create extreme physical conditions of ultrahigh-energy density in the laboratory. With multi-terawatt laser

Z. Gan · L. Yu · C. Wang · Y. Liu · Y. Xu · W. Li · S. Li · L. Yu · X. Wang · X. Liu · J. Chen · Y. Peng · L. Xu · B. Yao · X. Zhang · L. Chen · Y. Tang · X. Wang · D. Yin · X. Liang · Y. Leng · R. Li (✉) · Z. Xu

State Key Laboratory of High Field Laser Physics and CAS Center for Excellence in Ultra-Intense Laser Science, Shanghai Institute of Optics and Fine Mechanics(SIOM), Chinese Academy of Sciences(CAS), Shanghai 201800, China
e-mail: ruxinli@mail.siom.ac.cn

systems, focused intensities are mostly in the range of 10^{19} – 10^{21} W/cm². This ability opens for study particle (electron and proton) acceleration [1–4], x-/γ-ray generation [5–8] and plasma physics [9–12]. For the investigation of radiation reaction and quantum electrodynamics effects in plasmas, multi petawatt (PW) or even 100 PW laser systems are desired to achieve focused intensities over 10^{22} – 10^{24} W/cm² [13, 14].

Modern femtosecond high power lasers usually utilize MOPA (master oscillator power amplifier) configuration, with a mode-locked oscillator generated femtosecond few-cycle seed pulse, then a series of optical amplifiers to boost the output power. However, direct amplification of ultrashort laser pulse will produce very high peak intensities, resulting in detrimental nonlinear pulse distortion or even destruction of the gain medium. It was after the chirped pulse amplification (CPA) technique [15] was introduced in 1985 by Gérard Mourou and Donna Strickland that successful amplification of ultrashort laser pulse was achieved. By passing through a strongly dispersive element (the pulse stretcher, e.g., a grating pair or a long fiber) before amplification, the pulses are chirped and temporally lengthened to a much longer duration. This reduces the pulses peak power, avoids damage to the gain medium, and allows efficient energy extraction from the laser amplifier. After amplification, a compressor is used to remove the chirp and compress the pulses to ultrashort duration. The concept of CPA was then further extended by Audrius Dubietis in 1992 to present the method of optical parametric chirped pulse amplification (OPCPA) [16]. In contrast to CPA where amplification is based on stimulated emission in a laser gain medium, OPCPA transfers energy from a pump pulse to a stretched seed pulse through optical parametric amplification (OPA) in a nonlinear crystal.

CPA and OPCPA have become the standard solutions to build a petawatt class laser system. As showed in the reviews [17, 18], over 50 facilities that are, or have been, operational, under construction, or in the preparatory design phase around the world. Gérard Mourou and Donna Strickland have won the 2018 Nobel Prize in Physics due to their invention of the CPA technique, which made these high-intensity ultrashort lasers possible. After the discovery of ultra-broadband phase matching at the central wavelength of 910 nm can be achieved in the DKDP crystal [19, 20], which aperture can be 30 cm or even larger, several more ambitious projects are proposed to approaching 100–200 PW level outputs using OPCPA as the principal technique [17]. Of course, there is still a long way to overcome the 100 PW barrier. So many problems have yet to be solved, including high-quality large-aperture crystals, large compressor gratings, pump laser systems, and many more. Compared to OPCPA, the Ti:Sapphire (Ti:Sa) CPA technique has a number of important advantages such as higher stability and efficiency as well as lower requirements of the pump laser. These features make the Ti:Sa CPA technique the workhorse in most petawatt class laser systems with outputs of >1PW. The CPA technique is also thought to be on the verge of maturing to achieve 10-PW laser pulses output [21–23].

SULF (Shanghai Superintense Ultrafast Laser Facility) is a Ti:Sa CPA laser user facility built by a team from SIOM's (Shanghai Institute of Optics and Fine Mechanics) State Key Laboratory of High Field Laser Physics. SULF is located in a purpose-built building in the joint laboratory of SIOM and Shanghai Tech University.

The civil engineering construction started in December 2016 and has been completed in June 2018. In a neighboring building, the SULF prototype was constructed in early 2016 to carry out pre-research. Several important subsystems, such as high contrast front end, large-aperture Ti:Sa main amplifiers, dispersion control, wavefront correction and pump laser systems are verified by a performance test in the SULF prototype. SULF user facility began installation in August 2018, we upgrade 10 PW laser system based on pre-research in SULF prototype.

In this chapter, the SULF project is described. After introducing the structure of the SULF user facility, we focus on the SULF 10 PW laser system. The results of previous verified experiments in SULF prototype as well as the latest progress in SULF 10 PW laser user facility are presented. In the end, conclusions are drawn and prospects for future developments are discussed.

10.2 The Schematic Design of SULF

The laboratory structure of SULF is schematically illustrated in Fig. 10.1. It includes four major parts: laser systems, experimental end-stations, auxiliary facilities, and data center.

The laser system will deliver three beamlines: a 10 PW laser operated at 1shot/min, a 0.1 Hz 1 PW laser, and a 1 Hz 100 TW laser. Each laser has its own optical pulse compressor. The 10 PW laser and 1 PW laser are driven by a same oscillator with two parallel amplification arms. The 100 TW laser is generated by a beam splitter on the output port of the 1 Hz preamplifiers of the 10 PW laser. The three beamlines can be used independently or be used simultaneously in some particular experiments.

The laser system outputs, as well as the secondary radiation and particle sources driven by lasers, will be used in three experimental end-stations:

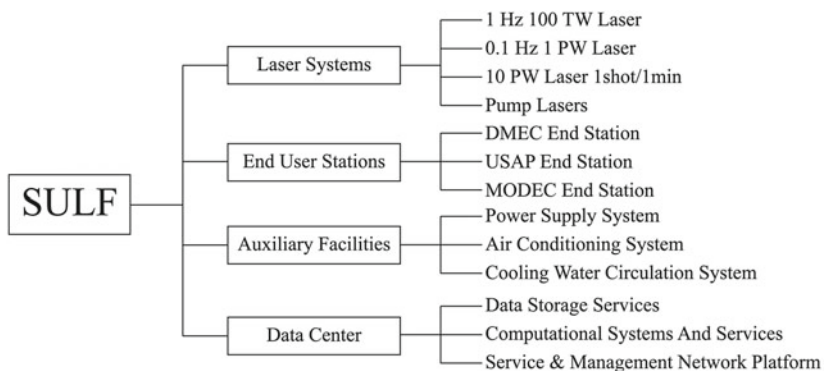


Fig. 10.1 The structure of SULF

- (1) DMEC (Dynamic of Materials under Extreme Conditions) end station. DMEC end station will allow researches such as high-order harmonic generation by intense ultrafast laser pulses, dynamic characteristics investigation of critical materials under extreme conditions, non-destructive testing of air materials or nuclear materials, etc.
- (2) USAP (Ultrafast Sub-atomic Physics) end station. USAP end station will allow researches such as accelerating charged particles (electrons and protons) to relativistic velocity, investigation of extreme phenomena in strong-field quantum electrodynamics, photonuclear physics, etc.
- (3) MODEC (Molecule Dynamics and Extreme-fast Chemistry) end station. MODEC end station will allow researches such as detection and control of chemical reactions, study of the structures, movements, and interactions of macromolecules, generating intense terahertz radiation, etc.

The auxiliary facilities include power supply systems, air conditioning systems, cooling water circulation systems, processing and testing equipment, etc. Auxiliary facilities provide necessary support and guarantee for the construction and daily operation of SULF.

The data center is set up to provide informational management of SULF. While realizing the efficient automatic operation of SULF, it can meet users' demands for real-time collection, transmission, processing, storage and sharing of experimental data.

10.3 The SULF 10 PW Laser System

The workhorse of the SULF facility is a 10 PW laser system. In a neighboring building, the SULF prototype was constructed in early 2016 to carry out pre-research and investigate the performance of the subsystems. SULF prototype achieved 5.4 PW output in the end of 2016 [23] and demonstrated 339 J energy output with a 235-mm diameter Ti:Sa CPA amplifier in 2017 [24]. The SULF building was completed in June 2018, the laser systems were then transferred into the new building and were reinstalled as SULF user facility. According to the pre-research experiment results in SULF prototype, we redesigned several subsystems and upgraded the whole 10 PW laser system.

Figure 10.2 shows the block diagram of the SULF 10 PW laser system. In the following section, the design of each subsystem and the upgrade information from SULF prototype to SULF 10 PW laser user facility are presented in detail.

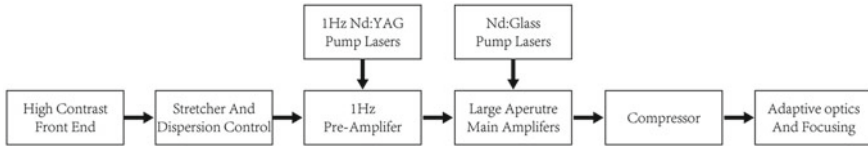


Fig. 10.2 Block diagram of the SULF 10 PW laser System

10.3.1 High Contrast Front-End

The focused peak intensity of the petawatt class laser pulse has now reached 10^{21} – 10^{22} W/cm², and may reach 10^{23} W/cm² in the near future [13, 14]. For experimental studies of the laser matter interaction with such high intensities, pre-pulse or amplified spontaneous emission (ASE) with intensities at the 10^{11} W/cm² level can generate significant unwanted pre-plasma on target [9]. Therefore, for focused laser intensity at 10^{21} W/cm², the temporal contrast should be better than 10^{-10} to limit destructive pre-plasma dynamics. At the intensities of 10^{22} W/cm² to 10^{23} W/cm², higher temporal contrast is required.

SULF 10 PW laser is based on double chirped pulse amplification (DCPA) with intermediate temporal pulse filtering. The first CPA stage is a commercial Ti:Sa laser system (Coherent, Astrella). Astrella can deliver a reliable output with pulse energy of 3.9 mJ and pulse duration <40 fs. The spectrum bandwidth and contrast ratio of the initial pulse from the Astrella is measured to be ~30 nm at full width at half maximum (FWHM) and $\sim 2 \times 10^{-8}$ at tens of picoseconds before the main pulse respectively. A novel pulse cleaning technique was developed in SULF prototype to generate high-contrast and broadband seed pulses for the second CPA stage.

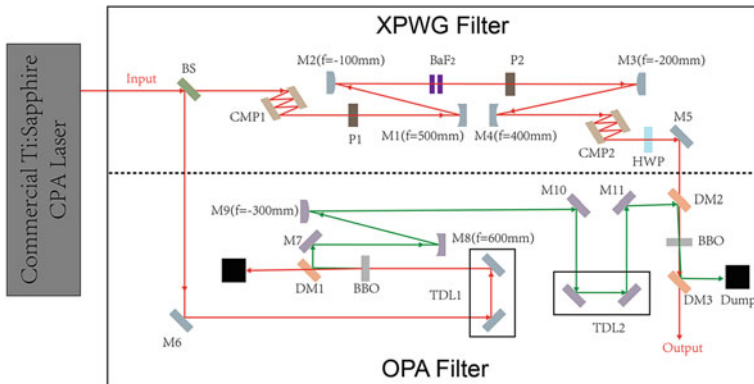


Fig. 10.3 Experimental scheme of the high contrast front end in SULF 10 PW laser. BS, beam splitter; M, mirror; CMP, chirped mirror pair; P, polarizer; DM, dichroic mirror; HWP, half wavelength plate; TDL, time delay line

Figure 10.3 shows the experimental scheme of the high contrast front end in the SULF 10PW laser, which combines cross-polarized wave generation (XPWG) and femtosecond OPA to generate high-quality clean seed pulses [25]. The Astrella output is divided into two laser beams by a beam splitter. The transmitted laser pulse with an $\sim 80 \mu\text{J}$ energy is the seed pulse for the XPWG filter, which is constructed using two BaF_2 crystals ([011]-cut orientation, 1.5 mm in thickness), two crossed polarizers with extinction ratios better than 10^5 , two sets of chirped mirrors and two telescopes. The BaF_2 crystals are placed in the air and are optimized to ensure good beam quality and long-term stability. After the first polarizer (P1), the seed pulse is focused by an all-reflective telescope (formed by M1 and M2). The second polarizer (P2) extracts the XPWG signal with a $9 \mu\text{J}$ energy output, which is then up-collimated by the second telescope (formed by M3 and M4). Two sets of chirped mirror pairs (CMP1 and CMP2) are used to compensate for the residual chirp introduced by optical components. The XPWG signal is then set to horizontally polarized by an achromatic $\lambda/2$ waveplate (HWP) and serves as the seed pulse for the subsequent femtosecond OPA.

The 3.82 mJ reflected laser pulse by beam splitter is frequency doubled by a 1-mm-thick beta-barium borate (BBO) crystal with 47% conversion efficiency. The second harmonic generation (SHG) pulse is separated by a dichroic mirror (DM1) and down-collimated by an all-reflective telescope (M9 and M10) to serve as the pump pulse in the femtosecond OPA stage. A 0.5 mm thick BBO crystal is used in the type-I phase matching OPA process. The SHG pump pulse and the signal pulse are synchronized by two time-delay-lines (TD1 and TD2) and combined by a dichroic mirror (DM2). The energy of the signal pulse after the DM2 decreases to $\sim 5 \mu\text{J}$, then it is amplified to $\sim 110 \mu\text{J}$ in the OPA process. The energy gain is more than 20 times. Consequently, the temporal contrast of the signal pulse is also promoted by more than 20 times. The energy fluctuation of the final clean pulse in one hour is as low as 1.8% (rms), and a smooth beam profile can be obtained in our experiment [25].

Spectral evolution in the front end is shown in Fig. 10.4. After the XPWG filter, the spectral bandwidth of the seed pulse was significantly enlarged, and the femtosecond OPA process further shapes the spectrum. The final clean pulse has a total bandwidth exceeding 60 nm (FWHM), nearly twice that of the initial pulse, which can support a Fourier-transform-limited pulse duration of 17 fs.

As shown in Fig. 10.5, The measured contrast ratio of the initial pulse from Astrella is approximately 2×10^{-8} at tens of picoseconds before the main pulse. Limited by the dynamic range of the measurement, the measured contrast ratio of the clean pulse is only $\sim 10^{-10}$ at several picoseconds before the main pulse. According to the extinction ratio of the polarizer (better than $10^5:1$) in the XPWG filter and the gain (~ 22 times) in the femtosecond OPA process, the temporal contrast enhancement should be about 6 orders of magnitude in theory. Correspondingly, the estimated temporal contrast of the final clean pulse should be 10^{-13} – 10^{-14} .

The above high contrast front end has been successfully demonstrated in the SULF prototype. The energy of the clean seed pulse was amplified to 7 J in 1 Hz pre-amplifier system, the measured contrast ratio was much better than 10^{-11} at 100 ps

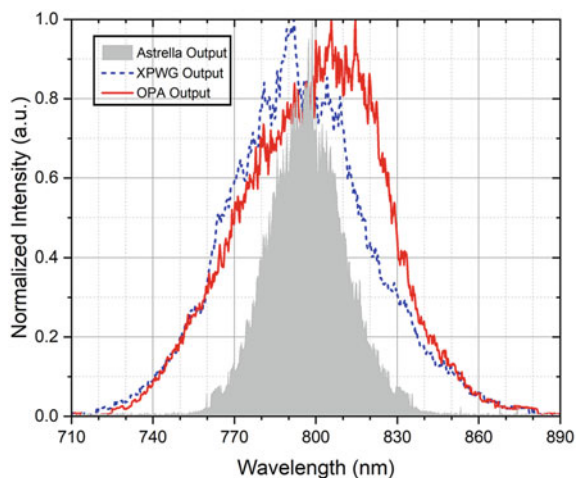


Fig. 10.4 Spectral evolution in the front end. Gray, initial pulse from Astrella; blue, output pulse from XPWG filter; red, femtosecond OPA output pulse

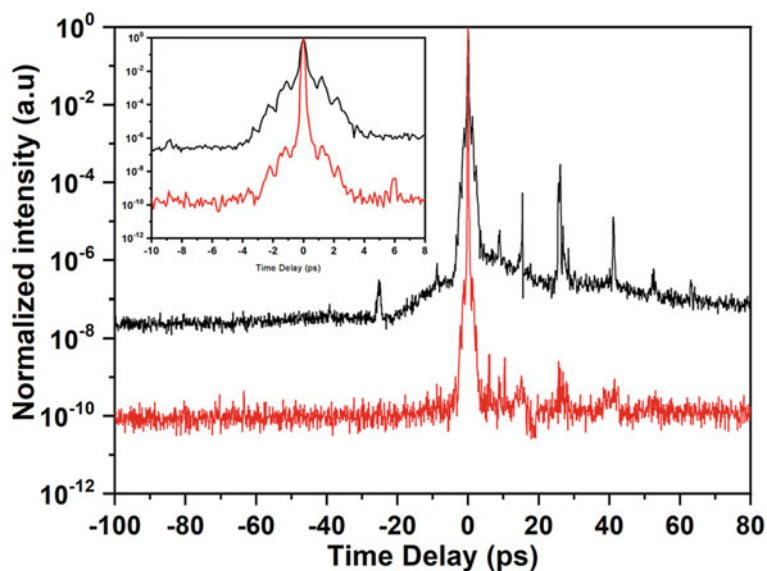


Fig. 10.5 Measured temporal contrast of the Astrella output pulse (black curve) and the final clean pulse (red curve). The inset shows the measured temporal contrast on the 18 ps scale

before the main pulse. We also used a single-shot third-order cross-correlator [25] to measure the temporal contrast of the large aperture main amplifier output with a pulse energy of about 50 J. The measured temporal contrast reached 10^{-10} level at 50 ps before the main pulse, which is the maximal dynamic range of the measurement tool. In SULF 10 PW laser user facility, a high contrast front end with the same structure is applied. The evolution of the pulse temporal contrast in the SULF 10 PW laser was investigated both theoretically and experimentally [26]. The study results provide the guideline for further improvement. We redesign several subsystems of SULF 10 PW laser, as shown in the following sections.

10.3.2 *Stretcher and Dispersion Control*

The CPA technique employs the concept of laser pulse stretching in the temporal domain and compression to ultrashort duration after laser pulse amplification. In SULF prototype, the high-contrast seed pulses were stretched to about 2 ns by a traditional Öffner stretcher before injected into the second CPA stage. The stretcher was designed as eight-pass configuration. The radii of curvature of the concave and convex mirrors are 1600 and 800 mm, respectively. The stretcher used a 1480 lines mm^{-1} , gold-coated grating with an incidence angle of 50° .

In PW laser systems, diffraction grating pairs are commonly adopted as a pulse compressor to compensate for the spectral phase distortions imposed by large amounts of optical components. The total group velocity dispersion (GVD) and third-order dispersion (TOD) of the laser system can be reduced to zero by adjusting the incidence angle and the slant distance of the gratings in compressor. For broadband laser pulse, the residual fourth-order dispersion over the required spectral range also needs to be compensated to achieve a Fourier-transform-limited pulse. In SULF prototype, a grism pair was utilized to control the high-order dispersion. The grism separation, angle of incidence and slant distance of the grating compressor were carefully controlled to compensate the dispersion up to fourth order. The 5.4 PW peak power recompressed pulse with a duration of 24 fs was obtained in the single-shot mode [27].

The Öffner stretcher and grism pair had played an important role in the SULF prototype. Due to the low grating efficiency, the transmission efficiency of the stretcher and the grism pair was measured to be only 28.5% and 10%, respectively. The study of pulse temporal contrast evolution in the SULF 10 PW laser indicates that the energy loss in the stretcher and grism pair will significantly degrade the temporal contrast of the laser system. Therefore, we redesign and upgrade the subsystem of stretcher and dispersion control in the SULF 10 PW laser user facility.

In SULF 10 PW laser system, grating in the standard Öffner stretcher will be ~ 375 mm from the center of the sphere. The spherical aberration cannot be neglected. It is also difficult to obtain a high-quality beam from the traditional One-grating Öffner stretcher when pulse spectrum broader than 100 nm. In SULF 10 PW laser user facility, a double-grating Öffner stretcher is adopted, as shown in Fig. 10.6.

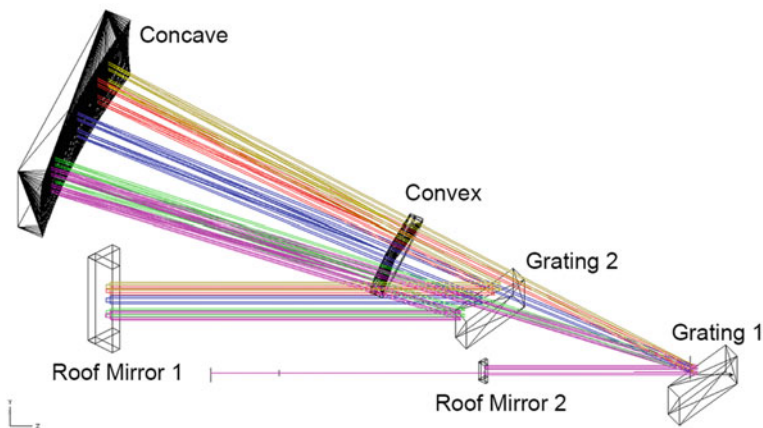


Fig. 10.6 Sketch of the double-grating Öffner stretcher at SULF user facility

Raytracing simulation and experimental study shows that the double-grating stretcher is absolutely aberration-free in both the near-field and far-field when properly aligned [28]. The transmission efficiency of the new stretcher is as high as 40%, which is 1.4 times the previous one.

In SULF 10 PW laser user facility, the grism pair is replaced by an acousto-optic programmable dispersive filter (Fastlite, Dazzler). The Dazzler can compensate for high-order phase distortions and shape the spectrum simultaneously at a higher transmission efficiency (~17%).

10.3.3 1 Hz Pre-amplifiers

In SUFL prototype, the stretcher output pulse was amplified in the regenerative amplifier (FA) with a spectral filter to shape the pulse spectrum and suppress gain narrowing. However, Inserting the spectral filter will increase the FA cavity loss, thus causing degradation of the temporal contrast. Figure 10.7 shows the layout of the new 1 Hz pre-amplifiers system in SULF 10 PW laser user facility. RA are removed from the laser system and all multi-pass amplifications are employed throughout. A Pockels cell (PC) assembly, which consists of two high extinction ratio polarizers and a DKDP PC, is used for pre-pulse suppression and change the pulse repetition rate of the Dazzler output to 1 Hz. The 1 Hz pulses are expanded to 2.5 mm diameter and injected into the first eight-pass amplifier (AMP I), which is pumped at both sides with a total pump energy of 80 mJ and can amplify the pulse energy to 6 mJ. The output pulses from AMP I are expanded to 6 mm diameter and then injected into the second six-pass amplifier (AMP II), which is designed to amplify the pulse energy to 70 mJ under pump energy of 260 mJ. A commercial Nd:YAG laser is used to pump both the AMP I and AMP II. The third (AMP III) and fourth (AMP

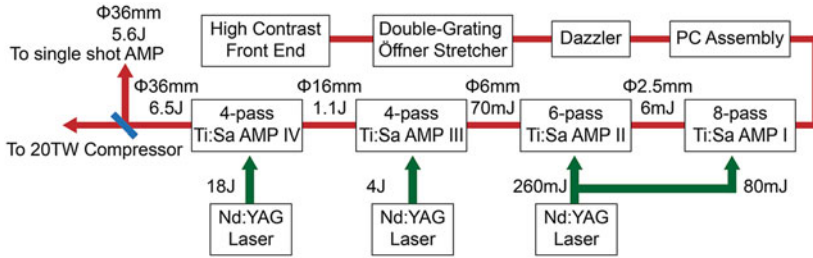


Fig. 10.7 Layout of the 1 Hz pre-amplifiers system

IV) amplifiers are both designed as four-pass configuration and double end pumped by home-built Nd:YAG lasers. The APM II output pulses are expanded to 16 mm diameter, the pulse energy is amplified to 1.1 J in AMP III under 4 J pump energy. Before injected into the AMP IV, the laser beam diameter is further enlarged to 36 mm. Beam homogenizers are applied in AMP IV to obtain a flat-top uniform pump beam profile. The laser pulse is amplified to 6.5 J under 18 J pump energy. The root mean square (RMS) stability of AMP IV output energy is measured to be 1.3% in one hour. The 5.6 J reflected laser pulse by beam splitter (BS) is directed to the single shot, large aperture main amplifiers. The beam profile and wavefront of the BS reflected laser pulse is shown in Fig. 10.8.

10.3.4 Large Aperture Main Amplifiers

To achieve a 10 PW peak power output from the SULF Ti:Sa CPA laser system, crystals with a diameter ≥ 200 mm are necessary for the final amplification stage. when designing such large aperture and high-gain amplifiers, a major challenge is to eliminate or relieve parasitic lasing (PL) effect and amplified spontaneous emission (ASE) [29–31]. PL is due to the formation of a laser cavity through Fresnel reflections at the material interfaces of the gain medium. ASE may place an even stronger restriction in large aperture amplifier, as it definitively increases with increasing pump energy, limiting the maximum stored energy. Flowing an index matching liquid around the crystal cylindrical surface can decrease the Fresnel reflection and increase the parasitic lasing threshold. For Ti:Sa crystals, di-iodomethane derivative (Series M, from Cargille Laboratories) is commonly used as the index matching liquid, which has an index of refraction close to 1.76 (the refractive index of Ti:Sa crystals). However, it is difficult to make sure exact index matching in whole gain bandwidth, as showed in Fig. 10.9. When multi-petawatt pulse output is desired, it is necessary to actively control the transverse gain during the pumping process. One idea is to carefully control the time delay between pump pulses and signal pulse, which is otherwise known as the extraction during pumping (EDP) technique [32]. Figure 10.10 shows the schematic of the EDP technique. In this method, the temporal delay between the

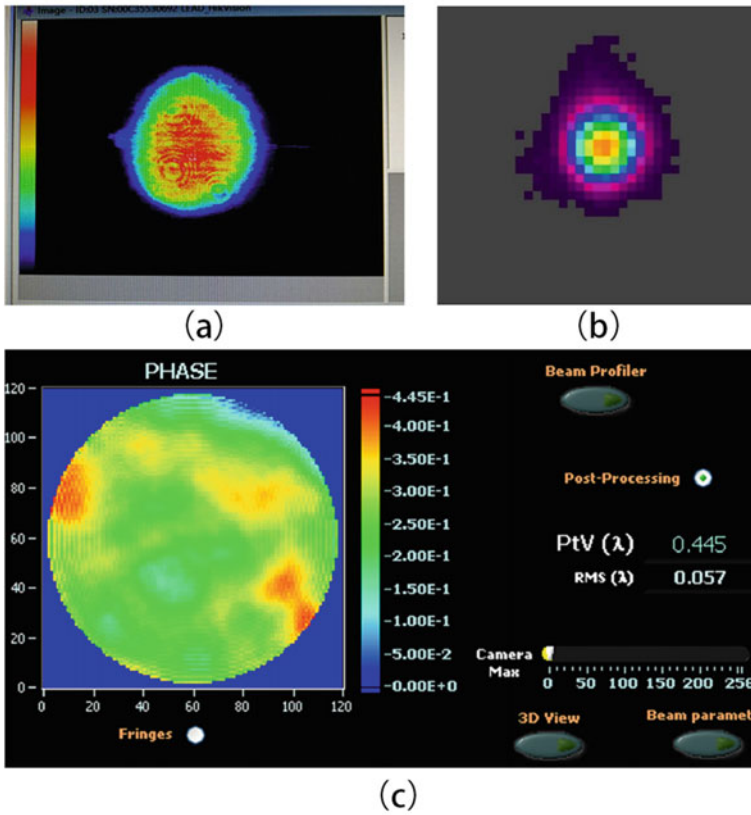


Fig. 10.8 Measured result of the reflected laser pulse by beam splitter **a** Near-field beam intensity profile; **b** Far-field beam intensity profile; **c** The wavefront phase profile

Fig. 10.9 Refractive index with respect to wavelength in different materials

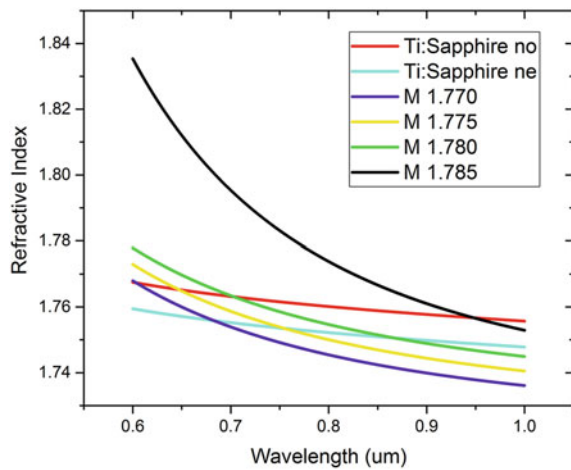
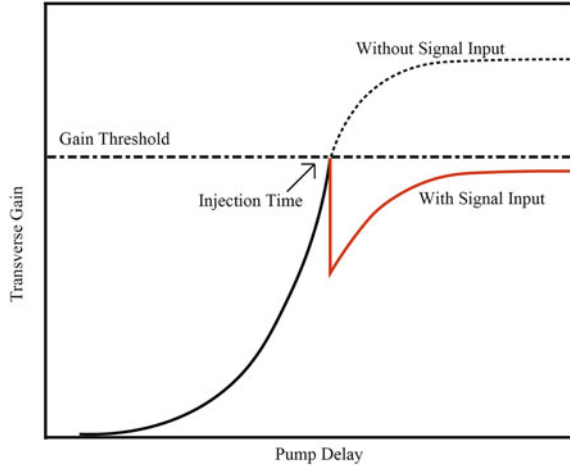


Fig. 10.10 Schematic of the extraction during pumping (EDP) technique



signal pulse and pump pulse is carefully controlled. Only part of the pump energy is stored in the gain medium before the arrival of the input signal. After signal pulse passes through the gain medium, stored energy transfers to the amplified signal pulse and the transverse gain rapidly decreases. The remaining pump pulses keep pumping for the next pass of the amplified signal pulse.

In SULF prototype, we successfully demonstrated 339 J energy output with a homemade 235-mm-diameter Ti:Sa crystal under 620 J pump energy [24]. The pump laser is a home-built frequency doubled Nd:glass disk amplifier which operated at a repetition rate of one shot every two hour. The pump-to-signal conversion efficiency of the final amplifier was only 32.1%. To increase the repetition rate and conversion efficiency of the amplifier, In SULF 10 PW laser user facility, the large aperture Ti:Sa amplifiers as well as their pump lasers are redesigned and upgraded.

Figure 10.11 shows the layout of the large aperture main amplifiers and pump lasers system in SULF 10 PW laser user facility. The 1 Hz pre amplifiers output laser beam is reshaped by a soft edge aperture with a 5 J energy output. The laser

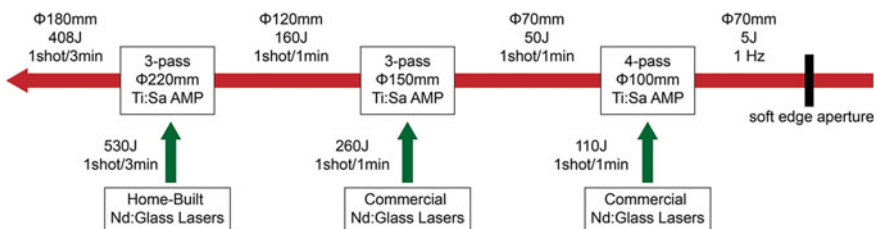


Fig. 10.11 Layout of the larger aperture main amplifiers and pump laser systems in SULF 10 PW laser user facility

beam is then expanded to 70 mm diameter and inject into a four-pass 100-mm-diameter Ti:Sa amplifier ($\Phi 100$ mm-AMP). The amplified signal pulse energy is 50 J under a pump energy of 110 J. The signal laser pulse is further expanded to a 120 mm diameter for the next injection into the three-pass 150-mm-diameter Ti:Sa amplifier ($\Phi 150$ mm-AMP). Signal pulse energy output of 160 J can be obtained when pump energy is 260 J. $\Phi 100$ mm-AMP and $\Phi 150$ mm-AMP are pumped by five commercial lasers (ATLAS 100, Thales). An ATLAS 100 laser can deliver two laser pulses with up to 50 J energy @527 nm in each pulse at a repetition rate of 1 shot/min. Prior to the injection into the final three-pass 220-mm-diameter Ti:Sa (GT Advanced Technologies) booster amplifier ($\Phi 220$ mm-AMP), the laser beam is enlarged to a diameter of 180 mm. $\Phi 220$ mm-AMP is pumped by six home-built high energy frequency-doubled Nd: glass lasers. Each home-built pump laser can deliver pump laser pulses with up to 100 J energy @527 nm at a repetition rate of one shot every three minutes.

To suppress the PL and ASE in $\Phi 220$ mm-AMP, a multi-pulse pump scheme is applied [23]. The pump energy absorption before the signal pulse arrival should be relatively large to ensure an adequate gain amplification. However, since the input signal energy is low, after the first-pass amplification, there remains a large degree of inversion population. The pump energy absorption between the first and second passes should refuel the consumed stored energy while avoiding overdriving the gain medium. Since the signal pulse energy increases after the first-pass amplification, a large amount of inversion population can be converted into signal pulse energy in the second-pass. The remaining pump pulses are absorbed by the gain medium to prepare for the third-pass amplification stage.

Figure 10.12 shows the measured output energies of $\Phi 220$ mm-AMP, the average output energy is 407.8 J at a pump energy of ~530 J. The RMS stability of the output energy is 0.8% in one and a half hours. The beam profile at the output of $\Phi 220$ mm-AMP is shown in Fig. 10.13.

Fig. 10.12 Measured output energies for 530 J pump energy in the final booster amplifier

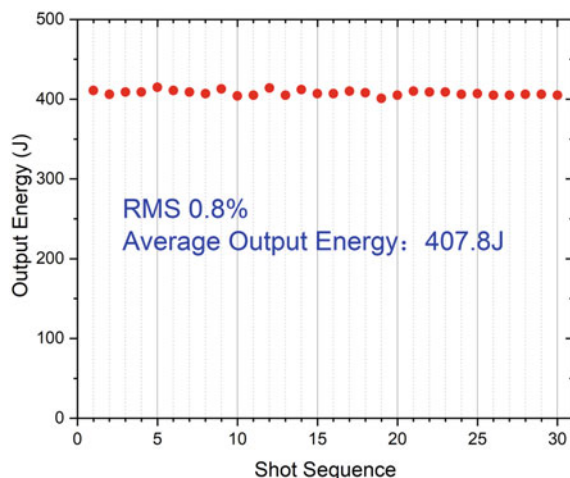
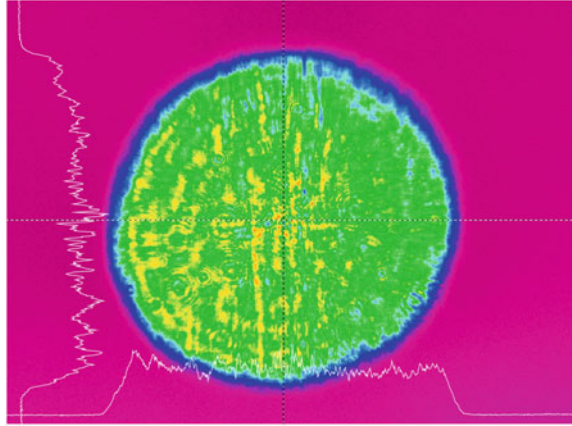


Fig. 10.13 Measured spatial beam profile of the amplified laser beam after the final booster amplifier



10.3.5 Compressor

The output pulses of $\Phi 220$ mm-AMP are transported from the ground floor to underground floor where the compressor is installed by a large aperture periscope. An achromatic image relay system is designed and installed to expand the beam size from $\Phi 180$ mm to $\Phi 500$ mm. The 10 PW compressor consist of four meter-size (575 mm \times 1015 mm) gold-coated gratings provided by Horiba, as shown in Fig. 10.14.

We use a commercial measurement device (Fastlite, Wizzler) to measure the characteristics of the recompressed pulse. Meanwhile, a Wizzler–Dazzler feedback loop system is used for dispersion control and optimize the compressed pulse duration.

The final spectrum, spectral phase and reconstructed compressed pulse shape are shown in Fig. 10.15. The FWHM duration of the compressed pulse is measured to be 22.4 fs. The total transport efficiency of the large aperture periscope, the achromatic image relay system and the grating compressor is measured to be 70.52%. The peak power of the final compressed femtosecond laser pulse is estimated to be 12.8PW (compressed pulse energy divided by the compressed pulse width).

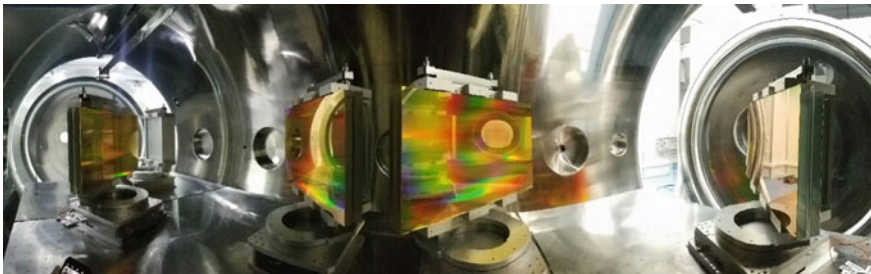


Fig. 10.14 SULF 10 PW grating Compressor

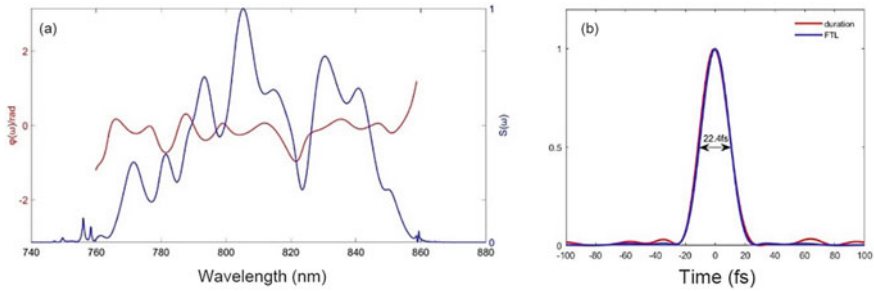


Fig. 10.15 **a** Spectrum and spectral phase of the amplified laser pulse; **b** Reconstructed compressed pulse with a 22.4 FWHM duration

10.3.6 Adaptive Optics and Focusing

Multi PW and even 10 PW lasers are very complex systems. To achieve an ultrahigh focus intensity, it is extremely crucial to correct the wavefront aberrations imposed by a lot of optical components. In the SULF 5 PW laser prototype experiment, we used cascaded double deformable mirrors (DMs) with different actuator densities to optimize the wavefront aberrations [13]. Typically, the first DM with a high spatial resolution compensates for small-scale high-order aberrations, and the second DM with a large stroke corrects large-scale low-order aberrations. In SULF user facility, we use a similar scheme to improve the focusing ability of the 10 PW laser system.

Figure 10.16 shows the layout of adaptive optics systems in the SULF 10 PW laser user facility. The wavefront distortion of the laser pulse is reduced to minimum by carefully controlling the quality of the optical components, the aberration of the beam expanders and the clamping stress of optical assemble. A bimorph DM with a diameter of 130 mm and 64 actuators was inserted after the 150-mm-Ti:Sa multi-pass amplifier, as the first wavefront corrector (DM1), as shown in Fig. 10.17a. The second DM (DM2) is installed after the grating compressor. DM2 has a clear aperture

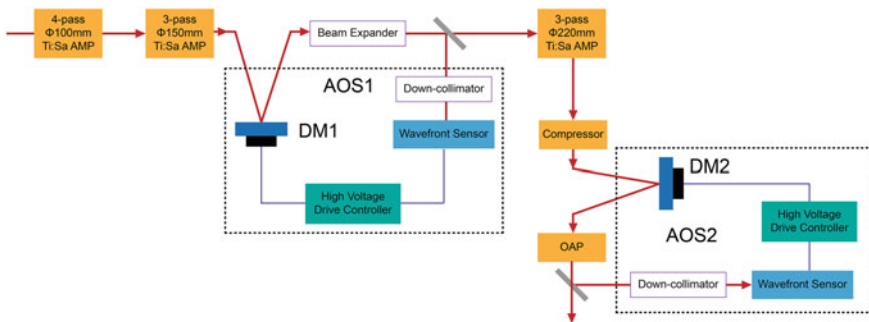


Fig. 10.16 Layout of adaptive optics systems in the SULF 10 PW user facility

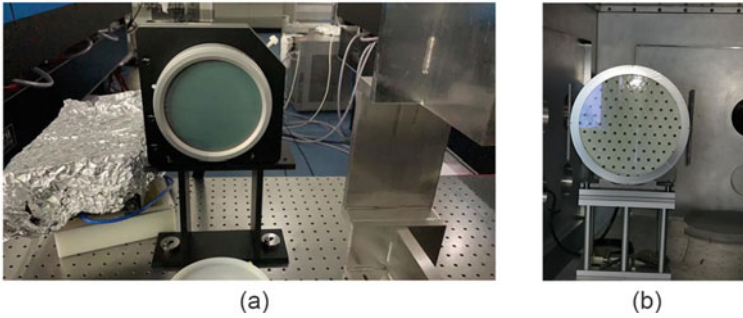


Fig. 10.17 **a** DM with a diameter of 130 mm and 64 actuators; **b** DM with a clear aperture of 500 mm and 121 actuators

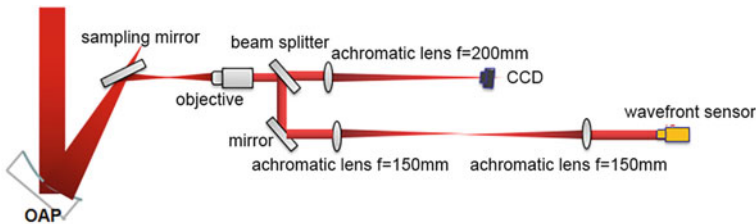


Fig. 10.18 The sampling optical path for wavefront sensor and far-field camera

of 500 mm and 121 actuators, as shown in Fig. 10.17b. After pass through the DM2, laser beam is focused in the target chamber using an $f/4$ off-axis parabolic mirror (OAP).

The wavefront distortions are compensated by cascaded double DMs in a closed feedback loop with the wavefront sensors. The sampling optical path for diagnostics is shown in Fig. 10.18. The phase profile of the laser beam before and after the correction are presented in Fig. 10.19a, b. There was a decrease in the PV and RMS values of the beam at the measured point from 2.663 μm and 0.686 μm to 0.261 μm and 0.052 μm . Far-field profile after the correction confirms the good focus ability of the beam as shown in Fig. 10.19d. The FWHM of the focal spot was $5.5 \times 5.5 \mu\text{m}^2$, which was close to the diffraction limit.

10.4 Conclusion and Outlook

In this chapter, we describe the structure of the SULF user facility and present the latest progress in SULF 10 PW laser system in detail. We improved the design of the SULF 10 PW laser user facility. A new double-grating stretcher and Dazzler are applied to decrease the energy loss of the high-contrast seed pulse. The RA

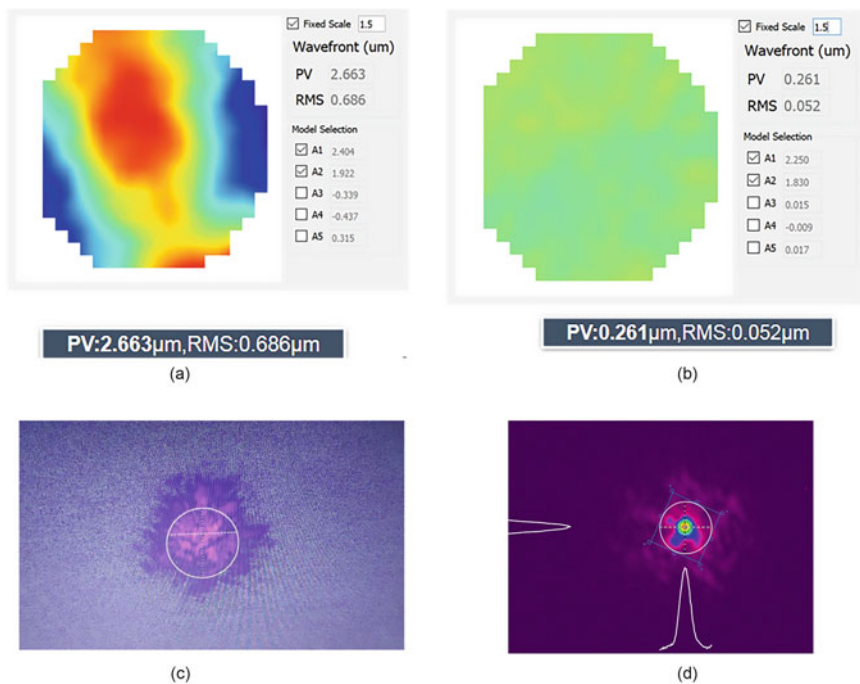


Fig. 10.19 Phase profiles measured after OAP by sampling optical path **a** before and **b** after the correction; **c** and **d** the corresponding focal spots focused by the OAP and obtained by an apochromatic objective lens (10×, Mitutoyo) and low-noise CCD

is replaced by an eight-pass pre-amplifier, which suffers a smaller energy loss and material dispersion and can support a higher temporal contrast during amplification. Large aperture main amplifiers and their pump lasers are redesigned and upgraded to increase the repetition rate to one shot every three minutes. The final Φ220 mm Ti:Sa amplifier output energy is measured to be ~408 J with an RMS stability of 0.8% in one and a half hours. By carefully controlling gain narrowing and high order dispersion, 22.4 fs FWHM duration of the full energy amplified laser pulse is obtained. The total transport efficiency of the large aperture periscope, the achromatic image relay system and the grating compressor is measured to be 70.52%. The peak power of the final compressed femtosecond laser pulse is estimated to be > 10 PW. In addition, good focus ability of the laser beam is confirmed by using cascaded double deformable mirrors with different actuator densities to optimize the wavefront aberrations.

Currently, the home-built Nd: glass pump lasers for the final Ti:Sa amplifier are under upgrade to increase the repetition rate to 1 shot/min. Temporal contrast measurement of the full energy amplified laser pulse is also under research.

References

1. W.T. Wang, W.T. Li, J.S. Liu, Z.J. Zhang, Z.Z. Xu, *Phys. Rev. Lett.* **117**, (2016)
2. J. Faure, Y. Glinec, A. Pukhov, S. Kiselev, S. Gordienko, E. Lefebvre, J.P. Rousseau, F. Burgy, V. Malka, *Nature* **431**, 541–544 (2004)
3. C.G.R. Geddes, C. Toth, J. van Tilborg, E. Esarey, C.B. Schroeder, D. Bruhwiler, C. Nieter, J. Cary, W.P. Leemans, *Nature* **431**, 538–541 (2004)
4. T. Tajima, J.M. Dawson, *Phys. Rev. Lett.* **43**, 267–270 (1979)
5. C. Yu, R. Qi, W. Wang, J. Liu, W. Li, C. Wang, Z. Zhang, J. Liu, Z. Qin, M. Fang, *Sci. Rep.* **6**, 29518 (2016)
6. S. Corde, K.T. Phuoc, G. Lambert, R. Fitour, V. Malka, A. Rousse, A. Beck, E. Lefebvre, *Rev. Mod. Phys.* **85**, 1–48 (2013)
7. M. Fuchs, R. Weingartner, A. Popp, Z. Major, S. Becker, J. Osterhoff, I. Cortie, B. Zeitler, R. Hoerlein, G.D. Tsakiris, U. Schramm, T.P. Rowlands-Rees, S.M. Hooker, D. Habs, F. Krausz, S. Karsch, F. Gruener, *Nat. Phys.* **5**, 826–829 (2009)
8. S. Kneip, C. McGuffey, J.L. Martins, S.F. Martins, C. Bellei, V. Chvykov, F. Dollar, R. Fonseca, C. Huntington, G. Kalintchenko, A. Maksimchuk, S.P.D. Mangles, T. Matsuoka, S.R. Nagel, C.A.J. Palmer, J. Schreiber, K.T. Phuoc, A.G.R. Thomas, V. Yanovsky, L.O. Silva, K. Krushelnick, Z. Najmudin, *Nat. Phys.* **6**, 980–983 (2010)
9. D. Umstadter, *Phys. Plasmas* **8**, 1774 (2001)
10. S.P.D. Mangles, C.D. Murphy, Z. Najmudin, A.G.R. Thomas, J.L. Collier, A.E. Dangor, E.J. Divall, P.S. Foster, J.G. Gallacher, C.J. Hooker, D.A. Jaroszynski, A.J. Langley, W.B. Mori, P.A. Norreys, F.S. Tsung, R. Viskup, B.R. Walton, K. Krushelnick, *Nature* **431**, 535–538 (2004)
11. Y.I. Salamin, S.X. Hu, K.Z. Hatsagortsyan, C.H. Keitel, *Phys. Rep.-Rev. Sect. Phys. Lett.* **427**, 41–155 (2006)
12. D. Umstadter, *J. Phys. D-Appl. Phys.* **36**, R151–R165 (2003)
13. Z. Guo, L. Yu, J. Wang, C. Wang, Y. Liu, Z. Gan, W. Li, Y. Leng, X. Liang, R. Li, *Opt. Express* **26**, 26776–26786 (2018)
14. J.W. Yoon, C. Jeon, J. Shin, S.K. Lee, H.W. Lee, I.W. Choi, H.T. Kim, J.H. Sung, C.H. Nam, *Opt. Express* **27**, 20412–20420 (2019)
15. D. Strickland, G. Mourou, *Opt. Commun.* **55**, 447–449 (1985)
16. A. Dubietis, G. Jonusauskas, A. Piskarskas, *Opt. Commun.* **88**, 437–440 (1992)
17. C.N. Danson, C. Haefner, J. Bromage, T. Butcher, J.-C.F. Chanteloup, E.A. Chowdhury, A. Galvanauskas, L.A. Gizzi, J. Hein, D.I. Hillier, N.W. Hopps, Y. Kato, E.A. Khazanov, R. Kodama, G. Korn, R. Li, Y. Li, J. Limpert, J. Ma, C.H. Nam, D. Neely, D. Papadopoulos, R.R. Penman, L. Qian, J.J. Rocca, A.A. Shaykin, C.W. Siders, C. Spindloe, S. Szatmari, R.M.G.M. Trines, J. Zhu, P. Zhu, J.D. Zuegel, *High Power Laser Sci. Eng.* **7** (2019)
18. C. Danson, D. Hillier, N. Hopps, D. Neely, *High Power Laser Sci. Eng.* **3** (2015)
19. V.V. Lozhkarev, S.G. Garanin, R.R. Gerke, V.N. Ginzburg, E.V. Katin, A.V. Kirsanov, G.A. Luchinin, A.N. Mal'shakov, M.A. Mart'yanov, O.V. Palashov, A.K. Poteomkin, N.N. Rukavishnikov, A.M. Sergeev, S.A. Sukharev, G.I. Freidman, E.A. Khazanov, A.V. Charukhchev, A.A. Shaikin, I.V. Yakovlev, *JETP Lett.* **82**, 178–180 (2005)
20. V.V. Lozhkarev, G.I. Freidman, V.N. Ginzburg, E.V. Katin, E.A. Khazanov, A.V. Kirsanov, G.A. Luchinin, A.N. Mal'shakov, M.A. Mart'yanov, O.V. Palashov, A.K. Poteomkin, A.M. Sergeev, A.A. Shaykin, I.V. Yakovlev, S.G. Garanin, S.A. Sukharev, N.N. Rukavishnikov, A.V. Charukhchev, R.R. Gerke, V.E. Yashin, *Opt. Express* **14**, 446–454 (2006)
21. D. N. Papadopoulos, J. P. Zou, C. Le Blanc, G. Cheriaux, P. Georges, F. Druon, G. Mennerat, P. Ramirez, L. Martin, A. Freneaux, A. Beluze, N. Lebas, P. Monot, F. Mathieu, P. Audebert, *High Power Laser Sci. Eng.* **4** (2016)
22. F. Lureau, S. Laux, O. Casagrande, O. Chalus, A. Pellegrina, G. Matras, C. Radier, G. Rey, S. Ricaud, S. Herriot, P. Jongla, M. Charbonneau, P.A. Duvochelle, C. Simon-Boisson, Latest results of 10 petawatt laser beamline for eli nuclear physics infrastructure, in *Solid state lasers xxv: Technology and devices*, ed. by W.A. Clarkson, R.K. Shori (2016)

23. Z. Gan, L. Yu, S. Li, C. Wang, X. Liang, Y. Liu, W. Li, Z. Guo, Z. Fan, X. Yuan, L. Xu, Z. Liu, Y. Xu, J. Lu, H. Lu, D. Yin, Y. Leng, R. Li, Z. Xu, *Opt. Express* **25**, 5169–5178 (2017)
24. W. Li, Z. Gan, L. Yu, C. Wang, Y. Liu, Z. Guo, L. Xu, M. Xu, Y. Hang, Y. Xu, J. Wang, P. Huang, H. Cao, B. Yao, X. Zhang, L. Chen, Y. Tang, S. Li, X. Liu, S. Li, M. He, D. Yin, X. Liang, Y. Leng, R. Li, Z. Xu, *Opt. Lett.* **43**, 5681–5684 (2018)
25. L. Yu, Y. Xu, Y. Liu, Y. Li, S. Li, Z. Liu, W. Li, F. Wu, X. Yang, Y. Yang, C. Wang, X. Lu, Y. Leng, R. Li, Z. Xu, *Opt. Express* **26**, 2625–2633 (2018)
26. L. Yu, Y. Xu, S. Li, Y. Liu, J. Hu, F. Wu, X. Yang, Z. Zhang, Y. Wu, P. Bai, X. Wang, X. Lu, Y. Leng, R. Li, Z. Xu, *Opt. Express* **27**, 8683–8695 (2019)
27. S. Li, C. Wang, Y. Liu, Y. Xu, Y. Li, X. Liu, Z. Gan, L. Yu, X. Liang, Y. Leng, R. Li, *Opt. Express* **25**, 17488–17498 (2017)
28. X. Liu, C. Wang, X. Wang, X. Lu, R. Li, *Optics* **1**, 191–201 (2020)
29. X. Liang, Y. Leng, C. Wang, C. Li, L. Lin, B. Zhao, Y. Jiang, X. Lu, M. Hu, C. Zhang, H. Lu, D. Yin, Y. Jiang, X. Lu, H. Wei, J. Zhu, R. Li, Z. Xu, *Opt. Express* **15**, 15335–15341 (2007)
30. F.G. Patterson, J. Bonlie, D. Price, B. White, *Opt. Lett.* **24**, 963–965 (1999)
31. V. Chvykov, J. Nees, K. Krushelnick **312**, 216–221 (2014)
32. V. Chvykov, K. Krushelnick, *Opt. Commun.* **285**, 2134–2136 (2012)